Numerical and Experimental Investigation of the Flow over a Car Prototype for the Shell Eco Marathon

F. Arpino[1], G. Cortellessa[1], A. Frattolillo[2], F. Iannetta[3]and M. Scungio[4†]

[1]*Department of Civil and Mechanical Engineering, University of Cassino and Southern Lazio, via G. di Biasio 43, 03043 Cassino (FR), Italy*
[2]*Department of Civil and Environmental Engineering and Architecture, Università degli Studi di Cagliari, Via Università 40, 09124 Cagliari, Italy*
[3]*L3 Calzoni, via A. De Gasperi 7, 40012 Calderara di Reno (BO), Italy*
[4]*Department of Economics, Engineering, Society and Business Organization, University of Tuscia, via del Paradiso, 47, 01100 Viterbo, Italy*

†*Corresponding Author Email: mauro.scungio@unitus.it*

ABSTRACT

The *Eco-Marathon* is a challenge organized by Shell in which student teams compete in designing energy-efficient vehicles. The event spark debate about the future of mobility and inspire engineers to push the boundaries of fuel efficiency. The aim of the present work consists of the numerical and experimental investigation of the aerodynamic performance of a *Shell Eco Marathon* prototype designed by a group of students of the University of Cassino, Italy. The car design has been provided by means of detailed 3D CFD modelling with Comsol Multiphysics®. The numerical tool has been validated against experiments conducted at the Laboratory of Industrial Measurements (LaMI) of the University of Cassino. In particular, a scale model of the car has been investigated in an open chamber wind tunnel by means of the *Particle Image Velocimetry* (PIV) technique, for different free stream velocities within the range 11 – 23 m/s. Measurements have been associated to a proper uncertainty analysis. The experimental data has been compared to numerical results obtained employing different turbulence models and the validated numerical tool has been applied to the simulation of the full-scale car model, allowing to analyse the wake flow structures, and estimate the overall drag coefficient.

1   INTRODUCTION

Energy saving and pollution issues are receiving growing concern in the modern transport engineering, pushing the automotive industry to develop innovative technologies to reduce gas emissions and fuel consumption. The realisation of highly efficient electric vehicles with very low fuel consumption can contribute to the reduction of environmental impact. Unfortunately, the development of this technology is slower than it could be (Ramos *et al.* 2014), but an attempt to raise awareness about high efficient electric cars is the organization of car competitions for students, in which the goal is to increase the energy efficiency of the vehicles instead of being the fastest, so the winning vehicle is the most energy efficient one.

Shell Eco Marathon (SEM) represents one of the most famous electric car contests, sponsored by the oil company Shell, and granted by the European Commission. SEM participants are asked to realize vehicles with the highest energy efficiency possible. The competition includes two categories: prototypes and urban concepts. While the only aim of participants to the former category is fuel consumption reduction of their vehicles, the urban concepts must be realized compliant to the criteria adopted for conventional road vehicles.

In the light of energy efficiency and fuel saving objectives, aerodynamic forces are of great interest for the decrease of resistance, and in particular for the drag force. The major contribution to aerodynamic drag arises from shape (or pressure) drag (Hucho *et al.* 1993). In the automotive industry, a survey of the scientific literature shows that even though in the last years the scientific research allowed a decrease of the drag force for commercial vehicles of almost 33%, a further improvement results to be challenging (Gupta *et al.* 1997; Kee *et al.* 2001).

The major contribution to a car's drag is due to the wake flow behind the vehicle. The location at which the flow separates determines the size of the separation zone, and consequently the drag force (Guilmineau (2008); Ahmed *et al.* (1984)) performed experiments with a bluff-body model, presenting pressure and force measurements, and wake surveys for different values of base-slant angle. They found that almost 85% of body drag is due to pressure drag, and most of this drag is generated at the rear end of the vehicle. They also showed that the value of the base slant-angle determines the strength and existence of the horseshoe vortices at the rear end of the model. In addition, Corallo *et al.* (2015) found that the aspect ratio of rear slant surface of an Ahmed-body geometry affects the flow structure and topology of the near wake, and has significant effect on the drag.

For a deeper understanding of the wake flow characteristics and of the separation process, which is essential for the accuracy of drag predictions, Computational Fluid Dynamic (CFD) analysis represents a powerful tool for the evaluation of vehicle aerodynamics because it can provide a large amount of information, difficult to obtain with experimental measurements (Arpino *et al.* 2014; Arpino *et al.* 2015a; Arpino *et al.* 2016; Massarotti *et al.* 2016). The most challenging aspect to reproduce in CFD simulations is the turbulent behaviour of the flow around the vehicles, which could be obtained through different modelling approaches. In practical applications, the steady state Reynolds Averaged Navier Stokes (RANS) modelling approach can be applied (Buonanno *et al.* 2003; Arpino *et al.* 2015b; Arpino *et al.* 2017a), even if more accurate and time-demanding modelling approach such as Large Eddy Simulation (LES) or Detached Eddy Simulation (DES) (Scungio *et al.* 2015a) are available. RANS modelling, in fact, has the limitation of not capturing the unsteady characteristics of a turbulent flow. Anyway, steady solution can be obtained if there is no characteristic large scale vortex shedding phenomenon (Regert *et al.* 2007). In addition, RANS approach can play a useful supplementary role of a wind tunnel test (Tsubokura *et al.* 2009).

The standard k-ε (Launder *et al.* 1974) and k-ω (Wilcox 2008) RANS models, which are claimed to satisfactorily reproduce separated turbulent flow characteristics, were used for the simulations of the present paper.

There are a lot of studies in scientific literature about RANS simulations of automotive aerodynamics. (Perzon *et al.* 2000) performed stationary simulations on the Asmo car model from Daimler-Benz, showing good agreement in pressure and prediction of drag coefficient. Musa *et al.* (2012) investigated the flow field around Ahmed body of a single cruising condition as the vehicle passes under a flyover, using a computational model based on RANS equation, while Bella *et al.* (2011) performed numerical investigation of flow around the Ahmed body with different slant rear angle configurations, using several RANS turbulence models. They evaluated the pressure drag, and other flow features such as flow structures and velocity field in the wake region, comparing them with experimental data and some prior RANS-based numerical studies. Majumder *et al.* (2014) studied the effects of fluid flow and the effective drag over a 3D standard vehicle, using the RANS equations with realizable k-ε turbulence model, evaluating and analyzing pressure, streamline contours, and velocity plots at rear part of the vehicle. Khalighi *et al.* (2012) investigated the aerodynamic flow field around a generic Sport Utility Vehicle using RANS simulations and experimental investigations with PIV technique, finding that the predicted drag coefficient was within 3-5% of the measured values.

The aim of the present work consists of the numerical and experimental investigation of the aerodynamic performance of a Shell Eco Marathon prototype, powered by a Proton Exchange Membrane Fuel Cell (PEMFC), accumulators and DC brushed motor, and designed by a group of students of the University of Cassino, Italy. To this aim, averaged velocity field measurements have been conducted on a 1:18 scaled model at the Laboratory of Industrial Measurements (LAMI) of the University of Cassino, employing an open chamber wind tunnel and the Particle Image Velocimetry (PIV) technique, already applied in our previous studies (Scungio *et al.* 2015b; Arpino *et al.* 2017b). Besides experiments, 3D numerical simulations have been performed and numerical results have been validated against experiments. The validated numerical model was then applied to the prediction of aerodynamic performance of the full-scale model and represents a useful tool for future optimization of the prototype shape aimed at further improvement of energy efficiency.

2   METHODS

2.1   The Nebula Prototype

In Figure 1 the Nebula car prototype is shown, which is a single-seater vehicle made up of a carbon fibre chassis and powered by a fuel cell system and a DC brushed motor. The prototype has 2700 mm of length, 598 mm of width, and 560 mm of height. Starting from the actual prototype, an accurate 1:18 scale model has been realised by means of a fused deposition modelling 3D printer. The scale model has 150 mm of length, 33 mm of width, and 31 mm of height. The scale model was used for experimental investigations in the wind tunnel, employing the PIV technique, and the experiments were numerically reproduced by means of 3D CFD simulations.
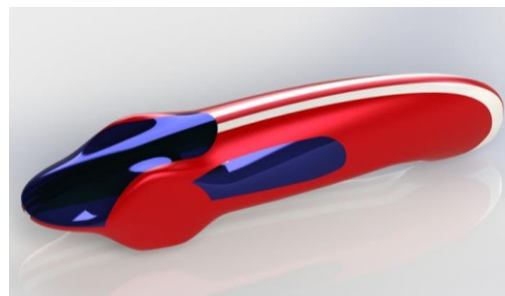

Fig. 1. Overview of the Nebula car prototype.

2.2 Wind tunnel and PIV system setup

The experimental investigations were performed in the wind tunnel of the Laboratory of Industrial Measurements (LaMI) of the University of Cassino and Southern Lazio (Italy) located in a 150 m^3 room having an ordinary mechanical ventilation system (air exchange rate equal to 0.3 h^{-1}) able to guarantee constant thermo-hygrometric conditions: temperature and humidity were kept constant at 20 ± 2 °C and 50 ± 5% RH, respectively.

The wind tunnel of the LaMI consists of an inlet nozzle (16:1 contraction ratio), flow conditioners (honeycombs), vortex generators, a flow establishment section, a test section, anti-swirl devices (honeycombs and grids) and a squirrel-cage centrifugal fan. A DC motor with a thyristor type control system maintains test-section wind speeds up to 25 m/s. Finally, the test chamber is of an Eiffel-type, with 1.1 m of height and 1.0 m of width.

The velocity field around the car prototype was characterized by means of the PIV measurement equipment available at the LaMI. The PIV technique is based on a simple principle: the flow is seeded by micron-sized particles and is illuminated twice by a laser light sheet in a very short time interval. Two images are obtained, from a special camera, when the particles are illuminated, and the local velocity vectors reconstruction is obtained from the two images over different interrogation areas via cross-correlation method (Keane *et al.* 2006). A sketch of the measurement domain adopted for the PIV tests in the wind tunnel available at the LaMI is reported in Figure 2, where details of the micron-sized particles are visible at the back of the model.
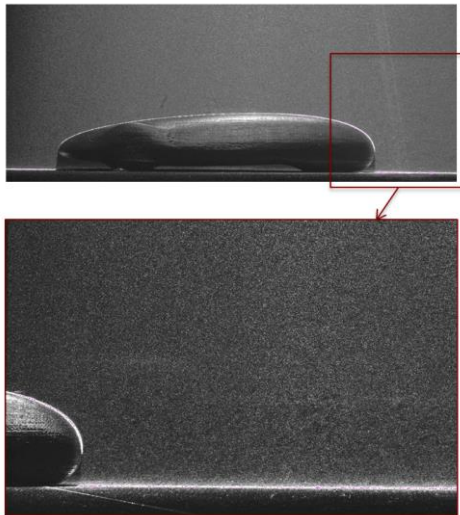
Fig. 2. Measurement domain adopted for the PIV analysis of the wake flow in the wind tunnel.

As the time interval is short compared to the flow time scales, the PIV method delivers instantaneous velocity maps in a two-dimensional plane (Stanislas *et al.* 1997). Details about such non-intrusive measurement technique are available in the scientific literature (Lazar *et al.* 2010; Adrian *et al.* 2011; Raffel *et al.* 2018) and are not reported here for brevity. The PIV measurements here described were obtained using a Litron Laser model NANO L135-15 and a camera TSI PowerView Plus model 7002262 equipped with 50 mm - 1:1.8 Nikkor optics, while the distance of the car model from the lens was equal to 555 mm and the lens aperture was set equal to 8.

In Table 1 the main experimental test parameters are resumed for the three reference wind velocities investigated. Detailed discussion about the significance of the parameters reported are available in literature (Bhattacharya *et al.* 2018).

2.3 Uncertainty Analysis of the PIV Measurements

An uncertainty analysis of the measured PIV data was provided on the basis of the well-known uncertainty propagation law (ISO/IEC Guide 98-3: 2008). For brevity, only a brief description of the procedure is reported.

The principle of the PIV measurement can be described by the following equation (Bhattacharya *et al.* 2018):

$$w = \alpha \frac{\Delta x}{\Delta t} + \delta w \tag{1}$$

where w is the velocity (m/s), Δx represents the pixel displacement of particles between PIV image pairs, δw (m/s) takes into account particle velocity lag from fluid acceleration together with three-dimensional effects on prospective of the velocity field, and α (m/pixel) is the scaling magnification factor.

The uncertainty affecting PIV velocity measurements can be calculated by means of the following propagation law:

$$u_w = \sqrt{\begin{array}{c} u_A^2 + \left(\dfrac{\partial w}{\partial \alpha}\right)^2 u_\alpha^2 + \left(\dfrac{\partial w}{\partial (\Delta x)}\right)^2 u_{\Delta x}^2 + \\ + \left(\dfrac{\partial w}{\partial (\Delta t)}\right)^2 u_{\Delta t}^2 + u_{\delta t}^2 \end{array}} \tag{2}$$

where u_w is the measured velocity standard uncertainty, u_A is the type A uncertainty, that for the case under investigation was evaluated to be negligible with respect to other uncertainty contributions, while u_α, $u_{\Delta x}$, $u_{\Delta t}$, $u_{\delta w}$ represent the standard uncertainties of different influence parameters. In particular, the standard uncertainty of the magnification factor, defined as $\alpha = \dfrac{l_r}{L_r}$, was evaluated by means of the following propagation law:

$$u_\alpha = \sqrt{\left(\frac{\partial \alpha}{\partial l_r}\right)^2 u_{l_r}^2 + \left(\frac{\partial \alpha}{\partial L_r}\right)^2 u_{L_r}^2} =$$
$$= \sqrt{\left(\frac{1}{L_r}\right)^2 u_{l_r}^2 + \left(-\frac{l_r}{L_r^2}\right)^2 u_{L_r}^2} \tag{3}$$

Where u_{l_r} and u_{L_r} were evaluated as the ratio between the resolution (in meters and pixels,

Table 1 Main test parameters of PIV measurements

	Uniform flow speeds, U_{REF} [m/s]		
	11	17	23
Target flow	2D air flow		
Measurement facility	Open chamber wind tunnel		
Measurement area	120×120 mm		
T_{REF}	28 °C		
Car prototype width, W	0.035 m		
Car prototype length, L	0.15 m		
Calibration			
Distance of reference points, l_R	170 mm	200 mm	200 mm
Distance of reference image, L_R	1697 pixels	1864 pixels	1864 pixels
Magnification factor, α	9.98 pixel/mm	9.32 pixel/mm	9.32 pixel/mm
Flow visualization			
Tracer generator	Stage-smoke generator (water-glycol droplets)		
1-min average particles diameter (mode), d_p	1.2 μm		
Light source	Double pulse laser		
Max laser power	135 mJ at 532 nm		
Thickness of the laser light sheet	$\cong 1.0$ mm		
Time interval, Δt	60 μs	45 μs	30 μs
Image detection			
Camera resolution	2048×2048 pixels		
Sampling frequency	7.25 Hz		
Distance from target, l_t	0.79 m	0.83 m	0.83 m
Prospective angle, θ	~ 6.5°		
Data processing			
Pixel unit analysis	Cross correlation method		
Correlation area size	32×32 pixels		

respectively) and $\sqrt{3}$ resulting in: $u_{l_r} = \dfrac{0.001}{\sqrt{3}} m$

and $u_{L_r} = \dfrac{1}{\sqrt{3}} pixel$. Similarly, the value of $u_{\Delta x}$ was evaluated as the ratio between the maximum error in the evaluation of *x*-displacement and $\sqrt{3}$ resulting in:

$$u_{\Delta x} = \frac{\left(1.2 \times 10^{-6}\right)}{\sqrt{3}} m \qquad (4)$$

Where the maximum error is evaluated as the mean diameter of the particles $\left(1.2 \times 10^{-6} m\right)$. Finally, $u_{\Delta t}$ was considered to be negligible with respect to the other uncertainty contributions.

A sensitivity analysis of mean velocity measurements, as a function of the number of acquisitions, was conducted up to 1250 PIV images, showing that the discrepancy in the averaged velocity is lower than 0.2% when the number of acquisitions is at least 250. As a consequence, in the present work uncertainty source related to Δt was considered negligible.

As a result of the uncertainty analysis, it was found that the composed velocity uncertainty, calculated assuming a coverage factor k=2 (confidence level 95%), was equal to 0.30 m/s, corresponding to 2.65 % for the first reference case (11 m/s), 0.4 m/s, corresponding to 2.35 % for the second reference case (17 m/s) and 0.6 m/s, corresponding to 2.55 % for the third reference case (23 m/s).

2.4 Mathematical and Numerical Models

The numerical simulations of the wake flow of the Nebula prototype were made by means of two RANS turbulence models, solved employing the commercial software Comsol Multiphysics®, already successfully applied our previous works (Scungio *et al.* 2015c; Scungio *et al.* 2016) In particular, the steady state, standard version of the *k-ε* model (Launder *et al.* 1974; Neft *et al.* 2016) and the Wilcox revised *k-ω* models (Wilcox 2008) were employed.

In Figure 3 the computational domain and the boundary conditions employed are reported. Given the symmetry of the geometry and boundary conditions employed, with respect to the mid-longitudinal plane (plane z-y) passing through the centre of the car model, only one half of the domain from the symmetry plane was considered. Such a simplification was allowed since the RANS modelling approach has been used for turbulence description, meaning that time-dependent and three-

dimensional velocity fluctuations due to turbulence are averaged in time.
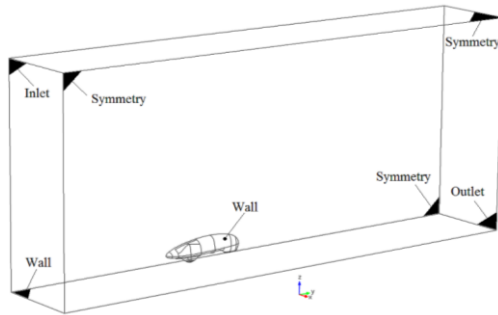
Fig. 3. Computational domain for the numerical simulations of the 1:18 scale model of the car prototype.

At the inlet, the y-component of the velocity was imposed, reproducing the same velocity profile as obtained from the PIV measurements, and placing the boundary condition at the same location as in the PIV experiments, which is equal to a distance of 300 mm from the front of the model. The outlet was placed at a distance of 450 mm from the back of the model, while on the base of the domain and on the model surface, a wall boundary condition was imposed (zero velocity condition). Finally, a symmetry condition was imposed on all the other sides. The whole computational domain has the dimensions of 500 mm of height (z-axis), 900 mm of depth (y-axis) and 200 mm of width (x-axis).

The maximum computational grid size in the free stream is equal to 20 mm. A grid refinement was made on the Nebula model surface and on the base of the domain (wall), using a minimum grid size of 1 mm with a growth rate of 1.3. The resulting unstructured computational grid is composed of about 3.8 million of tetrahedral elements. A grid sensitivity analysis was made by calculating the relative error between the vertical profiles of horizontal velocity obtained by two consecutive meshes, using a grid refinement factor of 1.5. With the proposed mesh, the mean relative error on the vertical profiles is maintained under 5%.

2.5 Drag Coefficient Calculation

The aerodynamic forces acting on a moving vehicle define a torsor of six components: drag, lift and lateral forces; rolling pitching and yawing momentum. The most important parameter in car aerodynamic study is the drag force, F_d, which is the force in the longitudinal flow direction, opposite to the vehicle movement.

Dimensionless drag coefficient could be defined as follow:

$$C_d = \frac{2 \cdot F_d}{\rho \cdot A \cdot V^2} \tag{5}$$

where ρ (kg/m^3) is the air density, V (m/s) is the air velocity and A (m^2) is the reference front vehicle surface.

There are two different contributors to the definition of the drag force: pressure force, which is due to a pressure difference across the surface; and viscous force, which is due to the friction acting in the opposite direction of the flow. In this paper, the drag force is numerically obtained by integrating the contribution from pressure and viscous forces on the vehicle surface, on four different sections of the vehicle: front-bottom, front-top, back-bottom and back-top (see Figure 4).

3 RESULTS AND DISCUSSIONS

### 3.1 Performance Analysis of the *k-ε* and *k-ω* Models

In this section, the performance of the two turbulence models is evaluated by numerically reproducing the wake flow and comparing the vertical and horizontal components of the averaged velocity with PIV measurements in the wind tunnel.

In Figures 5, 6 and 7 the results in terms of profiles of the horizontal and vertical components of the velocity are reported. The profiles, obtained with the *k-ε* and *k-ω* models, have been evaluated on the symmetry plane of the computational domain. On the same figures, a comparison with the data obtained from PIV analysis are reported in order to evaluate which turbulence model shows the better agreement with experiments.

Looking at the horizontal component of the velocity, from the Figures it could be observed that both the turbulence models are capable of reproducing the correct velocity profiles with almost the same performance at 11 m/s and 17 m/s. A little difference at that velocities could be observed on the upper side of the wake flow zone, in correspondence of the attachment between the recirculation vortex and the undisturbed flow, in which the *k-ω* model tends to slightly overestimate the velocity values. Greater discrepancies can be observed between the turbulence models under analysis at 23 m/s in the recirculation zone of the wake flow, where the *k-ε* model seems to have better performance in matching the experimental points of PIV measurements.

From an overall analysis of the figures 5, 6 and 7, it can be concluded that even if the two turbulence models adopted show comparable performance, the k-ε model results more suitable in reproducing the recirculating pattern of the wake flow in terms of horizontal component of the velocity.
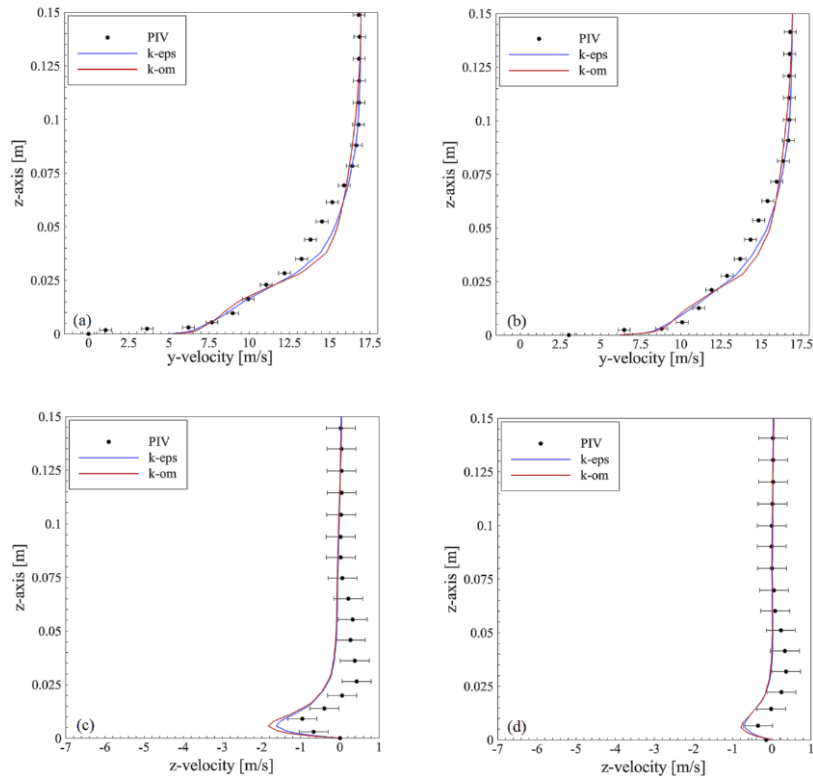
As regards the vertical component of the velocity reported in figures 5, 6 and 7, it can be observed that both the turbulence models under investigation show a slight difficulty to match the experimental measurements in the wake flow region behind the car, at L+45 mm, for all the wind speed considered. In particular, the magnitude of the vertical component of the velocity results overestimated in the wake flow, even if a little better performance can be attributed to the *k-ε* model. Slightly different behaviour can be observed with profiles evaluated at L+90 mm. In this case, the results from the two turbulence models are more accurate, with acceptable
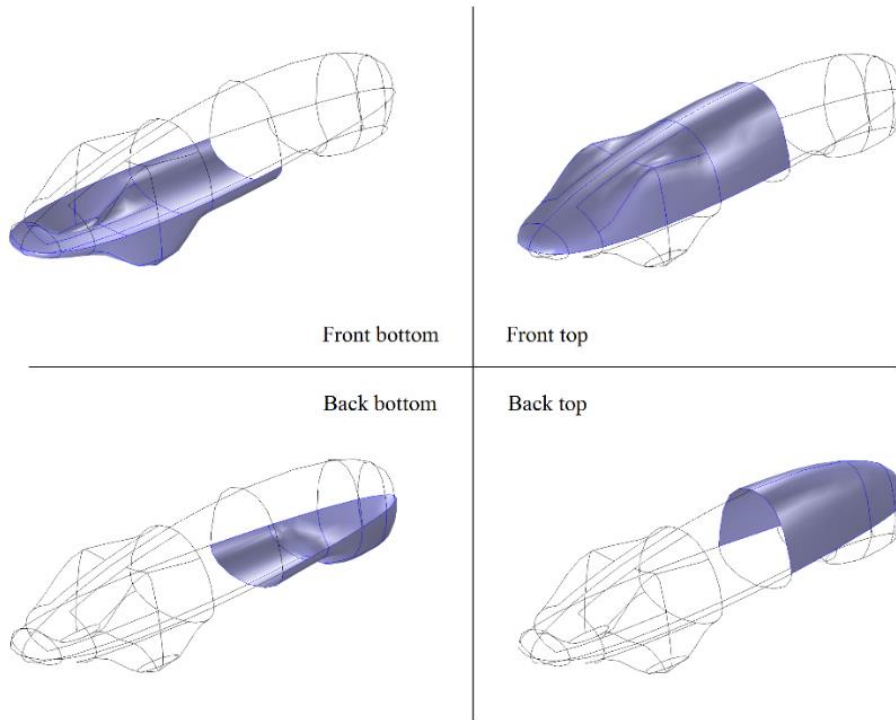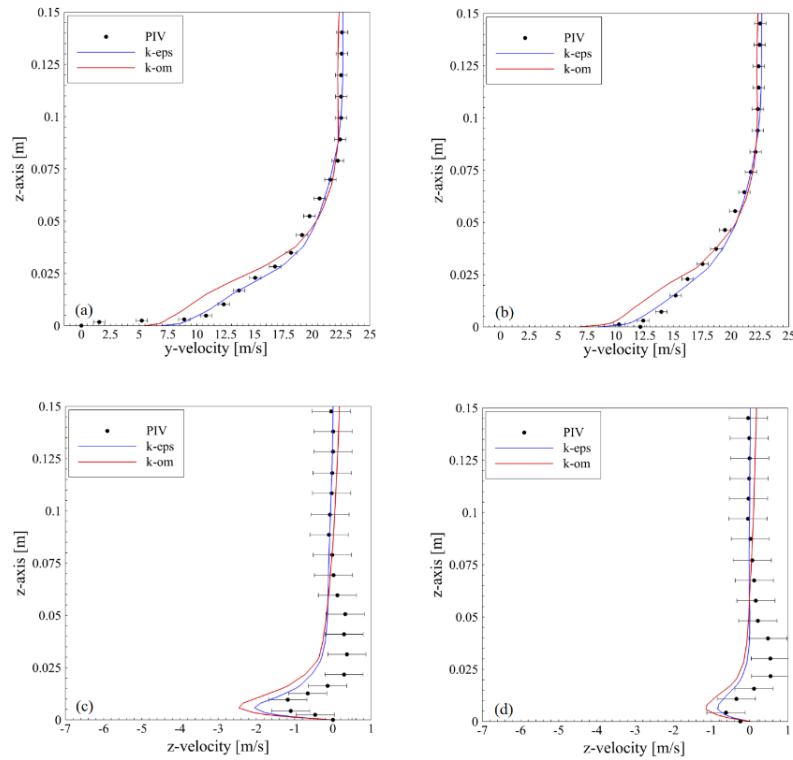
Fig. 4. Different sections of the vehicle surface for the calculation of the pressure and viscous forces.
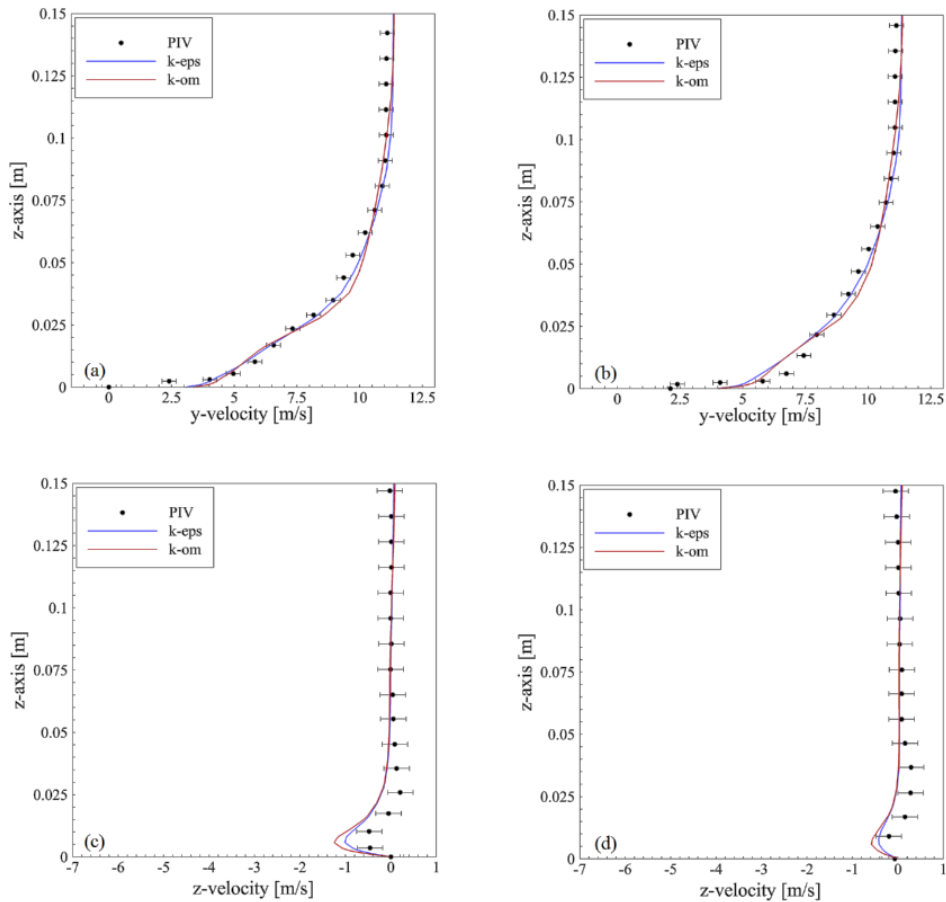
Fig. 5. Profiles of vertical and horizontal components of the velocity as obtained with the two-turbulence models adopted in the present simulations on the symmetry plane at 11 m/s: (a) and (b), horizontal component at L+45 mm and L+90 mm, respectively; (c) and (d), vertical component at L+45 mm and L+90 mm, respectively.

Fig. 6. Profiles of vertical and horizontal components of the velocity as obtained with the two-turbulence models adopted in the present simulations on the symmetry plane at 17 m/s: (a) and (b), horizontal component at L+45 mm and L+90 mm, respectively; (c) and (d), vertical component at L+45 mm and L+90 mm, respectively.

Fig. 7. Profiles of vertical and horizontal components of the velocity as obtained with the two turbulence models adopted in the present simulations on the symmetry plane at 23 m/s: (a) and (b), horizontal component at L+45 mm and L+90 mm, respectively; (c) and (d), vertical component at L+45 mm and L+90 mm, respectively.

Table 2 Viscous and pressure forces acting on the vehicle surface in the y-direction, calculated post processing the numerical data for different zones of the car model

	front-top	front-bottom	back-top	back-bottom	Total
Viscous force (N)	-0.129	- 0.110	- 0.079	- 0.051	- 0.369
Pressure force (N)	0.218	- 0.641	- 0.788	- 0.618	- 1.829
Total force (N)	0.089	- 0.751	- 0.867	- 0.669	- 2.198

precision for the farthest profile. In these cases, the difference between the k-ε and k-ω models decreases, even if a relatively better performance can be attributed to the k-ε model.

In conclusion, referring to the horizontal and vertical components of the velocity, the k-ε turbulence model results more suitable for the simulation of the wake flow behind the Nebula car prototype under investigation. Comparing the numerical results with the experimental measurements from PIV system, it can be concluded that the k-ε model shows a good capacity to reproduce the flow field and an overall better performance than the k-ω model.

3.2 Numerical analysis of the Wake flow – Simulation of the 1:1 Scale Model

Once analysed the performance of the turbulence models and verified the overall better performance of the k-ε model by comparing numerical results with PIV measurements in wind tunnel, a simulation of the full-scale Nebula car prototype has been realised in order to analyse the wake flow characteristics and to evaluate the drag coefficient of the car.

The computational domain is the same as for the previous simulations, but in this case the scale factor was set on the unity in order to study the car model in 1:1 dimensions. At the inlet, a constant horizontal component of the velocity was set equal to 13.9 m/s, reproducing a Nebula car moving at 50 km/h. No changes were made on the other boundary conditions.

In Table 2 the values of viscous and pressure forces acting on the vehicle surface in the y-direction, calculated post-processing the data obtained from the numerical simulation of the 1:1 car model, are reported. As can be seen, the greatest contribution to the drag force is due to the pressure force which has values higher than viscous component. It is noticeable that the pressure force on the front-top of the Nebula prototype results positive and then the total force in that zone acts in a direction which is in accordance to the vehicle movement. The total force acting on the bottom of the car surface (-1.42 N) results greater than that acting on the top (-0.778 N). The total force, including viscous and pressure components, results equal to 2.198 N, acting in a direction opposite to the vehicle movement, at 50 km/h.

Referring to equation (5) and calculating the reference front vehicle area, *A*, from geometrical data equal to 0.297 m², the drag coefficient of the Nebula prototype under examination, C_d, results equal to 0.066.

In Figure 8 the streamlines of the wake flow behind the Nebula prototype are reported: the streamlines colour is related to the velocity magnitude while their thickness is proportional to the turbulent kinetic energy. The zone corresponding to the base of the wake flow is characterized by thick streamlines, which means high turbulent kinetic energy, but low velocity magnitude. The same behaviour of low velocity magnitude and high turbulent kinetic energy could be observed at the wake flow behind the front wheels.
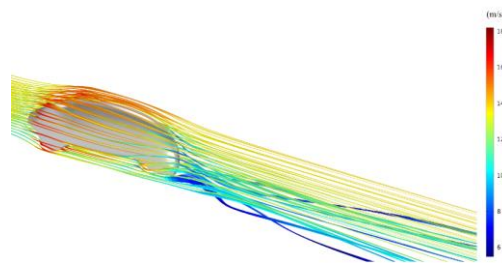
Fig. 8. 3D streamlines of the wake flow behind the Nebula prototype. The streamlines colour is related to the velocity magnitude and their thickness is proportional to the turbulent kinetic energy.

The higher value of the total force on the bottom of the car can be explained by looking at the streamlines around the car: on the upper surface of the model the flow results almost completely attached, while a recirculation zone characterizes the wake flow corresponding at the base of the model. Since the pressure drag force is very sensitive to shape and location of that recirculation regions, it is explained the greater value of the pressure drag force at the bottom of the Nebula prototype.

The same behaviour can be explained also looking at figures 9 and 10 that show the turbulent kinetic energy on the x-y plane, and the velocity vectors on a x-z plane at a distance of 0.15 m from the back of the car model. The figures confirm the presence of two counter rotating vortices at the base of the wake flow at the back of the vehicle.

This behaviour is in accordance with the Townsend's attached eddy hypothesis (A.A.Townsend 1976), whereby the flow structure consists of pairs of parallel vortex, which extract energy from the mean flow through the vortex stretching mechanism.

In addition, looking at figures 8 and 9, it can be observed that the two vortices are generated from a single point, as Townsend suggests, while Figure 8 confirms that the lower part of the vortices are bounded by the floor, which is supposed to reduce the overall size of the eddies.
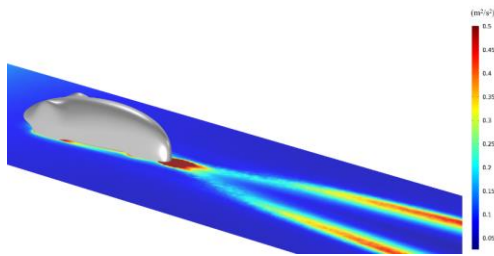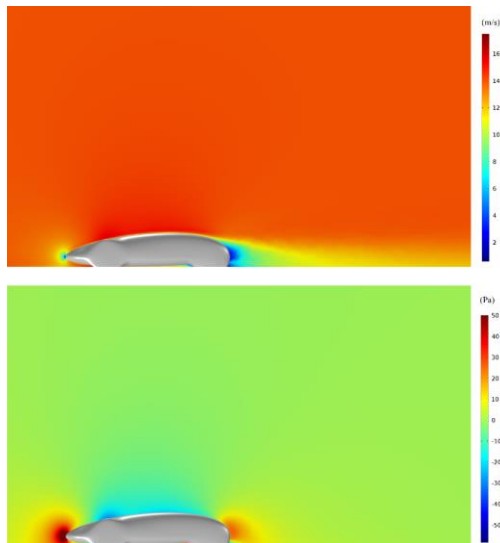
Fig. 9. Turbulent kinetic energy on the x-y plane, plotted at 12 cm from the base of the computational domain in the wake flow.
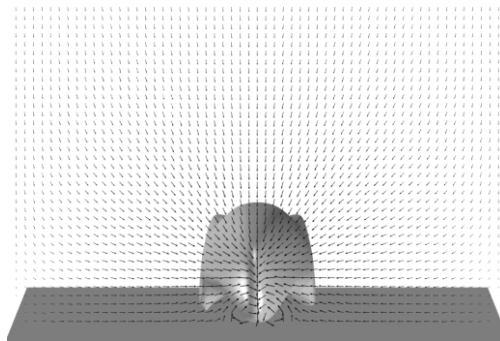
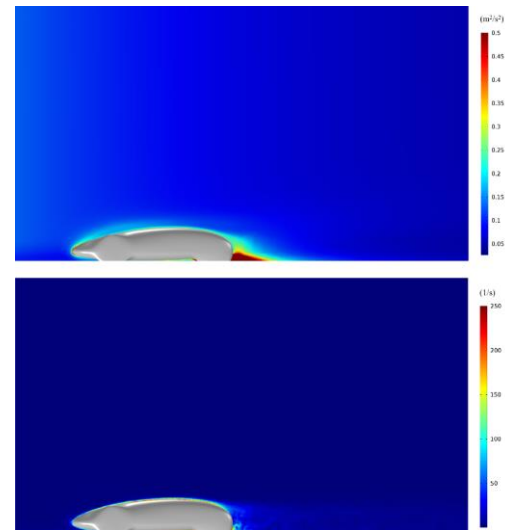**Fig. 10. Velocity vectors in the x-z plane at L+0.15 m.**

Fig. 11. Velocity magnitude (top) and pressure (bottom) fields around the Nebula model, on the symmetry plane of the 1:1 simulation case.

With the aim of Figure 11, that reports the velocity and pressure fields on the symmetry plane, it can be explained the vortex generation mechanism as the interaction of three behaviours: a high-speed stream along the side walls of the car, a slow speed zone at the back and a main flow along the top of the vehicle. The vortex structures in the wake flow are originated when the high-speed flow moving on the side wall of the car enters in the slow speed zone at the back. At this point the interaction with the main flow gives a twirling motion to the stream, changing its direction and creating the longitudinal vortices visible in figures 8 and 9.

One important factor affecting the aerodynamic drag, is the pressure gradient between the front and the back of the car. Figure 11 shows a high-pressure zone in the front of the car and a lower pressure zone at the back. Anyway, the low pressure zone at the back is characterized by relatively little low values (i.e. in comparison to what observed for Ahmed or Asmo bodies (Aljure *et al*. 2014)) which contributes to the reduction of the pressure gradient. This low-pressure gradient allows the flow to remain attached to the car surface, as observed in Figure 8.

In Figure 12 the turbulent kinetic energy (TKE) and vorticity magnitude on the symmetry plane are reported. As can be seen, the figure confirms the presence of a high TKE zone at the back of the car, immediately downstream at the rear wheel, where the two parallel vortices are generated, while lower values can be observed on the other zones of the car surface.

Fig. 12. Turbulent kinetic energy, TKE (top), and vorticity magnitude (bottom) fields around the Nebula model, on the symmetry plane of the 1:1 simulation case.

Looking at Figure 12, very few zones of high vorticity magnitude values can be observed: most of the vorticity is generated at the bottom and at the back of the car, in accordance with the previous behaviour, while the flow that results attached on almost the whole car surface, contributes to maintain a low value of vorticity on the vehicle surface.

Finally, in Figure 13 the profiles of vertical and horizontal components of the velocity are reported at different distances from the back of the car, on the symmetry plane. The figure allows to evaluate the development of the flow, in terms of velocity components, as the distance from the car increases. Looking at the horizontal component of the velocity, the nearest profile results very scattered, while the others become smoother as the distance from the car increases. On the contrary, the profiles of vertical component result very smooth for all the distances. In addition, the nearest profile of vertical component tends to maintain significant negative values, i.e.
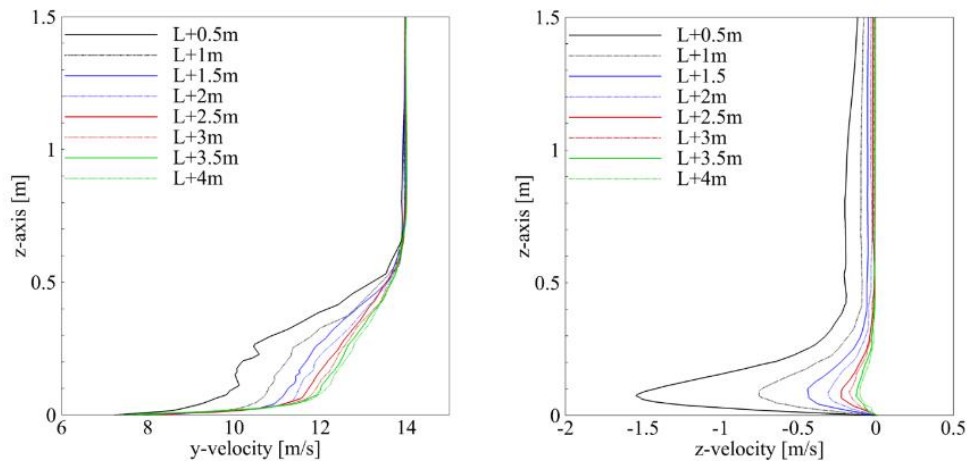
Fig. 13. Profiles of vertical and horizontal components of the velocity as obtained with the k-ε turbulence model at different distances from the back of the Nebula car, on the symmetry plane for the 1:1 simulation case.

descending flow, even at relatively high distance from the wall (at least up to 1.5 m).

4   CONCLUSIONS

In the present paper, numerical simulations of the wake flow behind a Shell Eco Marathon vehicle prototype, called Nebula, were carried out using RANS turbulence model and the commercial CFD software Comsol Multiphysics. In order to verify the suitability of the numerical model, results from k-ε and k-ω turbulence models, in terms of horizontal and vertical components of the velocity, were compared with experimental data from a wind tunnel investigation made out with Particle Image Velocimetry (PIV) technique. In order to experimentally analyse the wake flow characteristics with PIV method, a scale model of the Nebula prototype was realised by means of a 3D printer working on a fused deposition modelling (FDM) principle. The printed model was adequately studied in a closed-circuit wind tunnel facility available in the Laboratory of Industrial Measurement (LaMI) of the University of Cassino and Lazio Meridionale. Once verified which turbulence model is more suitable for the reproduction of the flow around the Nebula prototype, a 1:1 scale simulation was carried out in order to study the wake flow characteristics and roughly evaluate the drag coefficient.

From the numerical analysis, it was found that the most suitable RANS turbulence model for the simulation of the wake flow of the Nebula car is the standard k-ε model, which is able to correctly reproduce the horizontal velocity component of the wake flow, even if a little discrepancy with experimental data can be observed with the vertical velocity component.

A very low value of the drag coefficient, C_d, of the prototype under investigation was found (order of 10^{-2}). It was also found that the total force acting on the bottom of the car surface (-1.42 N) results greater than that acting on the top (-0.778 N), due to the formation of two recirculation vortices in the car wake flow, while the flow on the upper surface results almost completely attached.

From the numerical simulation, it was found an overall good performance of the Nebula prototype in terms of aerodynamic efficiency, finding a very low air resistance, comparable with other concept/experimental cars.

The results shown in this paper concern about a pre-design stage, which will be followed by more accurate CFD simulations (i.e. adopting DES and LES models for the numerical resolution of the turbulent flow structures) and experimental investigations (i.e. implementing a moving ground technique in order to evaluate the ground effect on the vehicle aerodynamics).

REFERENCES

Townsend, A.A. (1976). *The structure of turbulent shear flow*, Cambridge University Press.

Adrian, R. J. and J. Westerweel (2011). *Particle Image Velocimetry*. Cambridge University Press.

Ahmed, S. R., G. Ramm, G., Faltin (1984). Some salient features of the time-averaged ground vehicle wake. *SAE Technical Papers*. International Congress and Exposition, Detroit, United States, February-March.

Aljure, D. E., O. Lehmkuhl, I. Rodríguez, A. Oliva (2014). Flow and turbulent structures around simplified car models. *Computers and Fluids* 96: 122-135.

Arpino, F., A. Carotenuto, M. Ciccolella, G. Cortellessa, N. Massarotti, A. Mauro (2016). Transient natural convection in partially porous vertical annuli." *International Journal of Heat and Technology* 34(Special Issue 2): S512-S518.

Arpino, F., G. Cortellessa, Dell'Isola, M., Massarotti, N., Mauro, A. (2014). High order explicit solutions for the transient natural convection of incompressible fluids in tall cavities. *Numerical Heat Transfer; Part A: Applications* 66(8): 839-862.

Arpino, F., G. Cortellessa, M. Dell'Isola, M. Scungio, V. Focanti, M. Profili, M. Rotondi, (2017). CFD simulations of power coefficients for an innovative Darrieus style vertical axis wind turbine with auxiliary straight blades. *Journal of Physics: Conference Series* 923(1).

Arpino, F., G. Cortellessa, A. Frattolillo (2015a). Experimental and numerical assessment of photovoltaic collectors performance dependence on frame size and installation technique. *Solar Energy* 118, 7-19.

Arpino, F., G. Cortellessa, M. Ciccolella,G. Cortellessa, N. Massarotti, A. Mauro (2015b). Transient thermal analysis of natural convection in porous and partially porous cavities. *Numerical Heat Transfer; Part A: Applications* 67(6), 605-631.

Arpino, F., G. PeCortellessa, A. Frattolillo, M. Caschera, A. lliccio (2017b). Experimental and numerical investigation of the effects of wind exposure on historical towns. *Energy Procedia*. 133, 312-326.

Bella, G. and V. K. Krastev (2011). On the rans modeling of turbulent airflow over a simplified car model. *ASME-JSME-KSME 2011 Joint Fluids Engineering Conference, AJK 2011*.

Buonanno, G., A. Carotenuto, G. Giovinco, N. Massarotti (2003). Experimental and theoretical modeling of the effective thermal conductivity of rough steel spheroid packed beds. *Journal of Heat Transfer* 125(4): 693-702.

Corallo, M., J. Sheridan, M. C. Thompson (2015). Effect of aspect ratio on the near-wake flow structure of an Ahmed body. *Journal of Wind Engineering and Industrial Aerodynamics* 147: 95-103.

Guilmineau, E. (2008). Computational study of flow around a simplified car body. *Journal of Wind Engineering and Industrial Aerodynamics*. 96(6-7), 1207-1217

Gupta, A. and S. M. Ruffin (1997). Aerothermodynamic design of supersonic channel airfoils for drag reduction. *SAE Technical Papers*.

ucho, W. H. and G. Sovran (1993). Aerodynamics of road vehicles. *Annual Review of Fluid Mechanics*. 25(1), 485-537

ISO/IEC Guide 98-3:2008 (JCGM/WG1/100). Uncertainty of measurement - Part 3: Guide to the expression of uncertainty in measurement (GUM:1995).

Keane, R. D. and R. J. Adrian (2006). Theory of cross-correlation analysis of PIV images. *Appl. Sci. Res..* 49 (1992), 191-215

Kee, J. D., M. S. Kim, Lee, B. C. (2001). The COANDA flow control and Newtonian concept approach to achieve drag reduction of passenger vehicle. *SAE Technical Papers*. SAE World Congress, Detroit, MI, United States, March.

Khalighi, B., S. Jindal, and G. Iaccarino (2012). Aerodynamic flow around a sport utility vehicle-Computational and experimental investigation. *Journal of Wind Engineering and Industrial Aerodynamics* 107-108: 140-148.

Launder, B. E. and D. B. Spalding (1974). The numerical computation of turbulent flows. *Computer Methods in Applied Mechanics and Engineering*. 3(2), 269-289.

Lazar, E., B. DeBlauw, N. Glumac, C. Dutton and G. Elliott (2010). A practical approach to PIV uncertainty analysis. *27th AIAA Aerodynamic Measurement Technology and Ground Testing Conference 2010*.

Majumder, S. and S. Saha (2014). A method of drag reduction of a vehicle by computational investigation and geometric modification. *International Journal of Applied Engineering Research*. 9(6), 687-700

Massarotti, N., M. Ciccolella, G. Cortellessa and A. Mauro (2016). New benchmark solutions for transient natural convection in partially porous annuli. *International Journal of Numerical Methods for Heat and Fluid Flow* 26(3-4): 1187-1225.

Musa, M. N., K. Osman and A. M. A. Hamat (2012). Computational analysis of flow field around Ahmed car model passing underneath a flyover. *AIP Conference Proceedings*.

Neft, I., M. Scungio, N. Culver and S. Singh (2016). Simulations of aerosol filtration by vegetation: Validation of existing models with available lab data and application to near-roadway scenario. *Aerosol Science and Technology* 50(9): 937-946.

Bhattacharya, S., J. J. Charonko, P. P. Vlachos (2018). Particle image velocimetry (PIV) uncertainty quantification using moment of correlation (MC) plane. *Measurement Science and Technology* 29(11), article number 115301

Perzon, S. and L. Davidson (2000). On transient modeling of the flow around vehicles using the reynolds equation. *Int. Conference on Applied Computational Fluid Dynamics*. 720-727

Raffel, M., C. E. Willert, F. Scarano, C. J. Kähler, S. T. Wereley and J. Kompenhans (2018). *Particle Image Velocimetry, a practical guide*, Springer International Publishing.

Ramos, J. F., J. J. F. Lozanoand A. G. Caldero Én (2014). Design of electric racing vehicles: An experience of interdisciplinary project-based education in engineering. *2013 World Electric Vehicle Symposium and Exhibition, EVS 2014*.

Regert, T. and T. Lajos (2007). Description of flow field in the wheelhouses of cars. *International*

Journal of Heat and Fluid Flow. 28(4), 616-629

Scungio, M., F. Arpino G. Cortellessa and G. Buonanno (2015a). Detached eddy simulation of turbulent flow in isolated street canyons of different aspect ratios. *Atmospheric Pollution Research* 6(2): 351-364.

Scungio, M., F. Arpino M. Profili, M. Rotondi, V. Focanti and G. Bedon (2015b). Wind tunnel testing of scaled models of a newly developed Darrieus-style vertical axis wind turbine. *European Wind Energy Association Annual Conference and Exhibition 2015, EWEA 2015 - Scientific Proceedings*.

Scungio, M., G. Buonanno, F. Arpino and G. Ficco (2015c). "Influential parameters on ultrafine particle concentration downwind at waste-to-energy plants." *Waste Management* 38(1): 157-163.

Scungio, M., G. Buonanno, L. Stabile and G. Ficco (2016). Lung cancer risk assessment at receptor site of a waste-to-energy plant. *Waste Management* 56: 207-215.

Stanislas, M. and J. C. Monnier (1997). Practical aspects of image recording in particle image velocimetry. *Measurement Science and Technology.* 8(12), 1417-1426

Tsubokura, M., T. Kobayashi, *T. Nakashima, T. Nouzawa, T. Nakamura, H. Zhang, K. Onishi and N. Oshima* (2009). "Computational visualization of unsteady flow around vehicles using high performance computing." *Computers and Fluids* 38(5): 981-990.

Wilcox, D. C. (2008). Formulation of the k-ω turbulence model revisited. *AIAA Journal.* 46(11), 2823-2838.